

Noise Fusion-based Distillation Learning for Anomaly Detection in Complex Industrial Environments

Jiawen Yu¹, Jieji Ren², Yang Chang¹, Qiaojun Yu^{2,3}, Xuan Tong¹,
Boyang Wang¹, Yan Song¹, You Li¹, Xinji Mai¹ and Wenqiang Zhang^{1*}

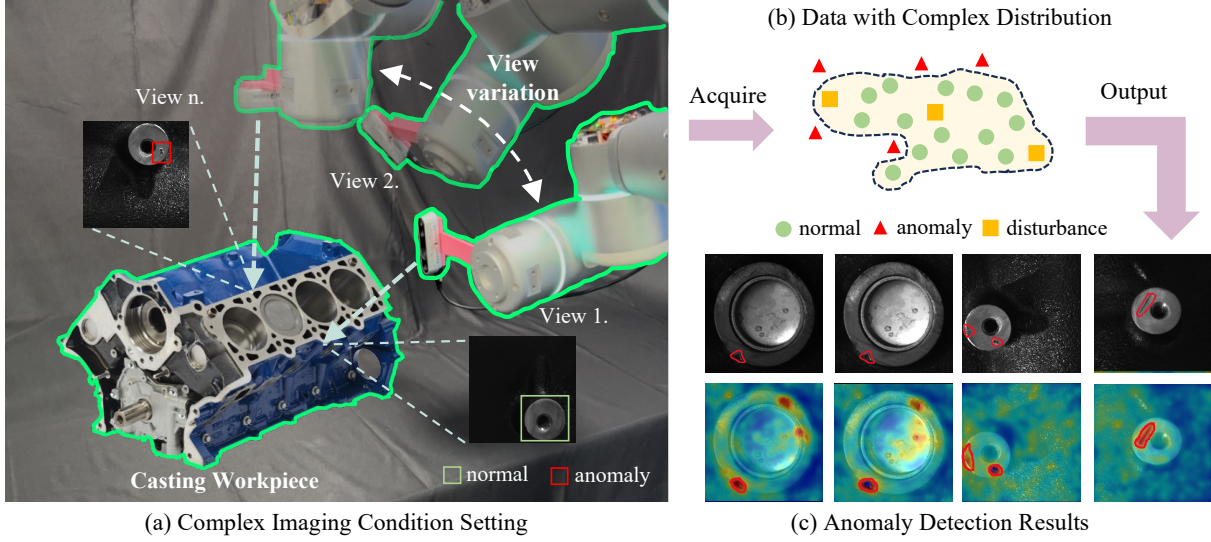


Fig. 1: (a) Illustration of our task setup. The moving robot arm introduces variations in imaging conditions like resolution, perspective and illumination. (b) Acquired image data exhibiting complex distribution, which presents challenges for models in distinguishing between normal and anomalous patterns. (c) Defects on casting workpieces in unstructured environments can be robustly highlighted by *HetNet*, enhancing production efficiency.

Abstract—Anomaly detection and localization in automated industrial manufacturing can significantly enhance production efficiency and product quality. Existing methods are capable of detecting surface defects in pre-defined or controlled imaging environments. However, accurately detecting workpiece defects in complex and unstructured industrial environments with varying views, poses and illumination remains challenging. We propose a novel anomaly detection and localization method specifically designed to handle inputs with perturbative patterns. Our approach introduces a new framework based on a collaborative distillation heterogeneous teacher network (*HetNet*), an adaptive local-global feature fusion module, and a local multivariate Gaussian noise generation module. *HetNet* can learn to model the complex feature distribution of normal patterns using limited information about local disruptive changes. We conducted extensive experiments on mainstream benchmarks. *HetNet* demonstrates superior performance with approximately 10% improvement across all evaluation metrics

on MSC-AD under industrial conditions, while achieving state-of-the-art results on other datasets, validating its resilience to environmental fluctuations and its capability to enhance the reliability of industrial anomaly detection systems across diverse scenarios. Tests in real-world environments further confirm that *HetNet* can be effectively integrated into production lines to achieve robust and real-time anomaly detection. Codes, images and videos are published on the project website at: <https://zihuatanejoyu.github.io/HetNet/>

I. INTRODUCTION

Defect detection serves as a cornerstone in manufacturing quality assurance, substantially improving production efficiency and product reliability [1], [2]. This capability is particularly essential for autonomous industrial systems that identify defects without human intervention [3]. The detection of surface anomalies on metal components—such as micro-cracks, porosity, or deformations—remains critical as these defects can compromise structural integrity and functional performance across automotive, aerospace, and precision machinery sectors [4], [5]. The unsupervised paradigm in anomaly detection holds substantial industrial value [6], as it circumvents the inherent challenges of limited defect samples and class imbalance, enabling more robust quality assurance in automated manufacturing processes.

*Corresponding author: Wenqiang Zhang.

¹Jiawen Yu, Yang Chang, Xuan Tong, Boyang Wang, Yan Song, Xinji Mai, You Li and Wenqiang Zhang are with College of Intelligent Robotics and Advanced Manufacturing, Fudan University, Shanghai, China. {jwyu23, ychang24, xtong23, bywang22, yansong24, youli22, xjmai23}@m.fudan.edu.cn, wqzhang@fudan.edu.cn

²Jieji Ren is with Shanghai Jiao Tong University, Shanghai, China. jiejiiren@sjtu.edu.cn

Qiaojun Yu is with ²Shanghai Jiao Tong University and ³Shanghai AI Laboratory, Shanghai, China. yqj11xs@sjtu.edu.cn

With the evolution of flexible manufacturing systems, traditional fixed-position inspection stations have become increasingly inadequate. This manufacturing paradigm shift has given rise to robot-based inspection systems that can adapt to varying product geometries and production layouts. However, robot-based inspection introduces significant challenges that current anomaly detection methods struggle to address. Contemporary approaches [7]–[13], while showing promising results in controlled environments [6], [14], exhibit diminished performance in real-world production settings [15]. These methods face critical limitations when confronted with uncontrolled illumination conditions, perspective variations, and magnification differences inherent to robotic inspection systems as illustrated in Fig. 1. Such environmental variables introduce significant intra-class variability and generate non-defective visual patterns that are frequently misclassified as anomalies, including specular reflections, motion blur, and inconsistent textural representations.

To address these fundamental challenges, we propose HetNet, a novel framework that models the complex manifold of normal patterns in unstructured inspection scenarios. Our approach is grounded in the principle that multi-modal feature extraction mechanisms can more effectively characterize the probabilistic distribution of normal variations—essential for robust anomaly detection in complex environments. By integrating CNN architectures (optimized for hierarchical local feature extraction) with Transformer networks (specialized in modeling long-range dependencies), we simultaneously capture heterogeneous features and local-global contextual information. This dual-representation approach effectively addresses the inherent trade-off between localization sensitivity and contextual reasoning. Our adaptive local-global feature fusion module employs a dynamic attention mechanism that optimizes information flow between complementary feature spaces, while our collaborative distillation framework enforces a joint optimization objective encompassing both reconstruction and denoising tasks. This approach guides the student network toward learning a more generalizable latent representation. Additionally, our local multivariate Gaussian noise generation module introduces perturbations in the feature space, effectively expanding the decision boundary to approximate natural variation limits of normal patterns.

Our main contributions are:

- A novel heterogeneous framework (HetNet) that leverages complementary feature extraction mechanisms to model complex normal variations in industrial environments with limited training data.
- An adaptive local-global feature (ALGF) fusion module with dynamic attention mechanisms bridging local sensitivity and global context awareness, and a local multivariate Gaussian noise (LMGN) generator that introduces structured perturbations approximating the natural variation boundaries of normal patterns.
- Extensive experiments on industrial benchmarks and real-world settings demonstrate robust performance improvements over existing approaches, particularly under varying environmental conditions.

II. RELATED WORK

This section briefly reviews anomaly detection methods and datasets. Various datasets used in the field of anomaly detection highlight different settings, data objects, and scales. These datasets have been leveraged in numerous approaches that address the task from different perspectives, which can be broadly categorized into embedding-based and reconstruction-based approaches.

A. Anomaly Detection Methods

Embedding-based methods rely on large-scale pretrained networks [16] to extract features, constructing distribution models of normal-class pretrained features [17]–[22] and identifying anomalies based on feature distance from the normal distribution. Other approaches use deep one-class classification models for single-class and novelty detection [23]–[26]. Methods based on knowledge distillation [27] employ a student network to learn from a pretrained teacher network on normal data, with output discrepancies used to localize defects [28]–[32]. Although embedding-based methods are computationally efficient due to the use of pretrained networks, they often exhibit lower detection accuracy.

Reconstruction-based methods utilize generative models to reconstruct images or pretrained features, aiming to detect anomalies through reconstruction errors [33]–[40]. Advanced models like GANs, Transformers, and Diffusion models [41]–[43] have been used to enhance reconstruction quality. The reverse distillation paradigm [30] introduces an encoder-decoder approach to increase representation discrepancies, further improved by subsequent works [44]–[46]. While these methods can achieve better localization accuracy, they depend heavily on the quality and quantity of training data, often leading to increased false positives when data is insufficient.

B. Anomaly Detection Datasets

Image anomaly detection datasets fall into two categories: synthetic and real-world objects. Synthetic datasets [47]–[49] are generated using computer-aided design software, which, while cost-effective and scalable, fail to capture natural factors like real camera distortions. Real-world datasets [6], [14], [50]–[56] focus on industrial parts, capturing images under controlled conditions, thus offering high-quality data. Given the importance of metal surfaces in industry, datasets specifically targeting metal defect detection [57]–[61] are crucial. However, these datasets are limited by their simplified lab environments, unlike the complexities found in real factories.

To bridge the gap between defect detection techniques and industrial environments, the MSC-AD dataset [15] was created, simulating multi-scene anomaly detection in real-world settings. With controlled light intensity and resolution settings, MSC-AD provides a realistic and challenging benchmark for evaluating industrial anomaly detection methods. Despite the critical role of metal surface defect detection in industrial production, it has not yet been thoroughly explored, highlighting the need for in-depth investigation.

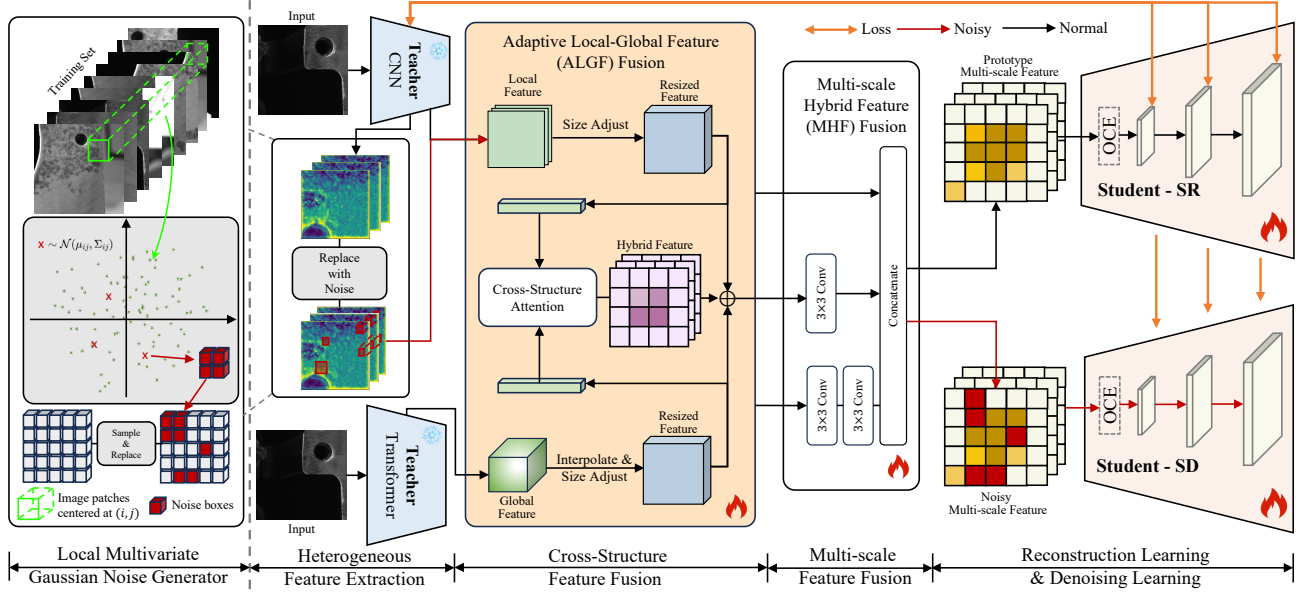


Fig. 2: The overall framework of HetNet. The heterogeneous teacher encoders initially extract pre-trained features, after which the Local Multivariate Gaussian Noise (LMGN) generator introduces noise before the features are passed to the ALGF module. Subsequently, cross-structural and multi-scale features are fused through the ALGF and MHF modules. The prototype and noisy multi-scale features are then sent to the student decoder for reconstruction and denoising training.

III. METHOD

A. Framework Overview

To address the challenge of avoiding misleading disturbances when detecting anomalies in complex industrial environments, the model should become more robust to highly variable inputs. Therefore, we propose the HetNet architecture, which learns complex normal pattern feature distributions containing local disruptive variations.

HetNet comprises four main components: a heterogeneous teacher network, a cross-structure feature fusion module, a multi-scale feature fusion module, and a collaborative student network. The image is input into two heterogeneous encoders to obtain local and global representations. The ALGF module fuses these features, facilitating effective interaction between global and local characteristics. The MHF module then combines features from different layers, passing them to the student decoder. The collaborative student more accurately model the normal patterns by denoising and reconstruction.

The following sections describe the heterogeneous teacher encoder, the hybrid feature fusion strategy, and the collaborative learning with local noise. The cross-structure and multi-scale feature fusion modules will be discussed together in the hybrid feature fusion strategy.

B. Heterogeneous Teacher Encoder

Existing reverse distillation methods often result in false positives in unpredictable environments, primarily due to their reliance on convolutional neural networks (CNNs) with limited receptive fields that overemphasize local features and are sensitive to abrupt changes. To mitigate these issues, we employ CNNs and Transformer networks as teacher networks

to capture both local details and long-range dependencies, making the model robust to local perturbations.

In HetNet, the Transformer teacher network T_{Trans} extracts global feature information, while the CNN teacher network T_{CNN} focuses on local feature representation, crucial for detecting small anomalies. Both networks are pretrained on ImageNet [62] with their parameters frozen during training.

Mathematically, let I represent the original input image, and the corresponding layer features in our heterogeneous teacher encoders are represented as $\{f_{\text{Global}}^k = T_{\text{Trans}}^k(I), f_{\text{Local}}^k = T_{\text{CNN}}^k(I)\}$, where T_{Trans}^k and T_{CNN}^k denote the k^{th} encoding layers in the Transformer and CNN, respectively. Here, $f_{\text{Global}}^k \in \mathbb{R}^{C_{\text{Trans}}^k \times H_{\text{Trans}}^k \times W_{\text{Trans}}^k}$ and $f_{\text{Local}}^k \in \mathbb{R}^{C_{\text{CNN}}^k \times H_{\text{CNN}}^k \times W_{\text{CNN}}^k}$, where C , H , and W represent the number of channels, height, and width of the feature maps. For the subsequent knowledge distillation, we need to fuse these feature maps from different sources. First, the smaller-sized Transformer feature map is resized via interpolation to match the dimensions of the corresponding CNN feature map, resulting in the new $\hat{f}_{\text{Global}}^k \in \mathbb{R}^{C_{\text{Trans}}^k \times H_{\text{CNN}}^k \times W_{\text{CNN}}^k}$.

C. Hybrid Feature Fusion Strategy

Different architectures capture distinct feature properties: CNNs focus on local details, while Transformers excel at modeling long-range dependencies. To effectively integrate these complementary representations, we propose a dynamic hybrid feature fusion strategy.

Our strategy comprises two modules: the Adaptive Local-Global Feature (ALGF) fusion module and the Multi-Scale Hybrid Feature (MHF) fusion module. ALGF operates at each layer, performing local-global cross-structural attention fusion to generate hybrid features. These hybrid features

are then further fused through MHF, resulting in multi-scale hybrid features.

Within a single ALGF block, we first align two teacher network feature channel numbers with convolution blocks and flatten them to get $f_{Local}^{tk}, f_{Global}^{tk} \in \mathbb{R}^{C^k \times H^k \times W^k}$.

Before flattening, we concatenate the two heterogeneous features along the channel dimension to obtain $g^k \in \mathbb{R}^{2C^k \times H^k \times W^k}$ for subsequent residual connection. Next, we use the feature f_{Local}^{tk} as the query and value, and f_{Global}^{tk} as the key to perform cross-structure attention. We then apply a convolution to increase the channel size and reshape the output:

$$h^k = \text{Conv}(\text{Attention}(f_{Local}^{tk}, f_{Global}^{tk}, f_{Local}^{tk})). \quad (1)$$

Finally, the output feature h^k from the attention module is added to the concatenated feature g^k , and a convolution is applied to further fuse these features, resulting in the output hybrid feature:

$$o^k = \text{Conv}(h^k + g^k) \in \mathbb{R}^{C^k \times H^k \times W^k}. \quad (2)$$

After independently computing o^k for multiple layers, where $k \in \{1, 2, \dots, n\}$, we further apply the MHF module to fuse multi-scale hybrid features, making the features passed into the bottleneck structure more compact and enriched. Specifically, similar to the approach in [30], shallow features are downsampled using one or more 3×3 convolutional layers with a stride of 2, followed by batch normalization and ReLU activation. The resized features from each layer are then concatenated. The output of the hybrid feature fusion is the prototype multi-scale feature o .

D. Collaborative Learning with Local Noise

Current reverse distillation methods rely on information-rich training data, but their generalization ability is limited when disturbance patterns are scarce, leading to reconstruction errors and false positives. To address this, we introduce collaborative distillation, where the student network performs both reconstruction and denoising tasks simultaneously. This improves feature quality and enhances robustness to normal disturbances. The noise for denoising is generated by a Local Multivariate Gaussian Noise (LMGN) generator.

Let the prototype multi-scale feature o be input into the student network SR^k for direct reconstruction, and the noisy multi-scale feature o' be input into the student network SD^k for denoising. We will discuss the process of constructing noisy feature o' later. These two student networks share parameters and each contains an OCE bottleneck module as in [30], as well as a decoder with the same structure as the teacher CNN but reversed. The activations of the student network are denoted as $\{f_{SR}^k = SR^k(o), f_{SD}^k = SD^k(o')\}$, collectively referred to as f_S^k . Following standard practice [27], [30], we compute the vector-wise cosine similarity loss along the channel axis between the CNN teacher network f_{Local}^k and the student network f_S^k , obtaining a 2-D anomaly

map $M^k \in \mathbb{R}^{H_{CNN}^k \times W_{CNN}^k}$. The objective functions are computed as:

$$L_{KD/Recon} = \sum_{k=1}^K \left\{ \frac{1}{H_k W_k} \sum_{h=1}^{H_k} \sum_{w=1}^{W_k} M_{SR/SD}^k(h, w) \right\}, \quad (3)$$

where k indicates the number of feature layers used in the experiment. The overall loss is defined as:

$$L_{Total} = L_{KD} + \alpha L_{Recon}, \quad (4)$$

where α is a regularization parameter.

To construct the noisy multi-scale feature o' mentioned above, we design a new LMGN generator to introduce normal disturbance information into the training features. Inspired by [19], we use a multivariate Gaussian distribution to describe the probabilistic representation of each position for the normal class and sample noise from this normal distribution to simulate complex normal variation patterns. We first use the CNN teacher network T_{CNN}^k to extract pretrained features from all images in the training set and take the feature vectors at the same center position (i, j) for all images, describing the normal feature distribution at different center positions (i, j) . At each center position (i, j) , we calculate the mean μ_{ij} and covariance Σ_{ij} following [19].

During training, we sample a noise of random size $\xi \sim \mathcal{N}(\mu_{ij}, \Sigma_{ij})$ from the above distribution and add it into features extracted from the teacher network f_{Local}^k . This process introduces local scale noise at different center positions of the feature map to obtain the final noisy feature, which is then fed into the subsequent ALGF module. The multivariate Gaussian distribution describes the distribution of normal features in the training set, and the noise sampled from this distribution is related to the normal features but has some randomness, enabling the student network to be more robust to slight variations that may exist in the input.

IV. EXPERIMENTS

We validated our method through extensive experiments on the MSC-AD dataset [15], demonstrating its effectiveness in complex environments. Additional tests on the MVTEC-AD, VisA and MPDD datasets [6], [54], [63] confirmed its generalization ability and robustness. Real-world environment tests further substantiated its practical application.

A. Experiments on the MSC-AD Dataset

1) Training Details:

Similar to [30], we use WideResNet50 [64] as the CNN encoder. Given the efficiency requirements in industrial defect detection, we selected the lightweight Swin-T-22k [65] as the Transformer encoder, resizing images to 256 resolution and utilizing the intermediate layers with $k = \{1, 2, 3\}$. We employed the Adam Optimizer [66] with betas=(0.5, 0.999), setting the learning rate to 0.005, and the regularization parameter of L_{Recon} to 0.1. We trained for 200 epochs with a batch size of 16.

2) Inference Details: During the inference stage, we maintain the overall framework but discard the LMGN generator. We extract the corresponding layer representation pairs from

TABLE I: Anomaly detection and localization results in terms of Image-AUROC / Pixel-AUROC / Pixel-AUPRO on the MSC AD dataset. Best results in **bold**, N indicates the unavailable results.

Condition		DRAEM [35]	CFA [26]	CFLOW [21]	RD4AD [30]	HetNet(Ours)
Resolution	150x150	54.40 / 77.39 / N	65.34 / N / 85.65	52.33 / 87.03 / 60.80	42.62 / 86.24 / 69.86	83.31 / 97.42 / 93.34
	200x200	57.08 / 80.17 / N	73.68 / N / 88.62	60.71 / 88.50 / 62.54	48.88 / 90.01 / 76.81	88.94 / 98.40 / 96.01
	300x300	57.07 / 82.21 / N	66.62 / N / 88.01	53.00 / 86.84 / 65.94	42.42 / 89.96 / 77.37	85.57 / 98.09 / 94.95
	600x600	47.01 / 87.10 / N	63.78 / N / 87.49	60.35 / 90.56 / 66.49	41.30 / 91.21 / 78.10	85.41 / 97.98 / 94.55
Illumination	high	50.86 / 81.81 / N	67.12 / N / 87.10	52.73 / 87.44 / 63.30	42.53 / 89.70 / 76.75	83.18 / 97.68 / 94.77
	mid	56.49 / 81.67 / N	68.75 / N / 87.53	56.85 / 88.51 / 63.94	43.54 / 89.55 / 76.16	86.62 / 98.17 / 94.89
	low	54.32 / 81.68 / N	66.19 / N / 87.78	60.21 / 88.75 / 64.33	45.35 / 88.80 / 73.69	87.62 / 98.05 / 94.48
Surface	back	20.11 / 83.10 / N	51.62 / N / 88.97	32.01 / 86.71 / 49.28	38.33 / 91.04 / 78.40	73.16 / 96.55 / 93.19
	down	69.80 / 89.84 / N	72.94 / N / 92.40	65.44 / 89.11 / 72.53	41.90 / 90.44 / 74.60	87.30 / 98.30 / 95.37
	front	88.69 / 91.29 / N	88.88 / N / 96.55	69.90 / 9.87 / 76.55	54.80 / 92.58 / 82.36	93.30 / 99.36 / 97.39
	left	44.25 / 65.89 / N	71.30 / N / 89.71	45.53 / 87.10 / 54.47	37.75 / 83.98 / 72.23	89.89 / 98.11 / 92.26
	right	42.91 / 72.38 / N	54.63 / N / 88.60	43.53 / 83.97 / 58.64	36.76 / 87.08 / 68.02	78.20 / 97.47 / 95.96
	up	57.57 / 87.82 / N	64.75 / N / 68.58	83.16 / 88.65 / 72.86	53.30 / 91.01 / 77.60	93.00 / 98.03 / 94.11
<i>Total Average</i>		53.89 / 81.72 / N	67.35 / N / 87.47	56.60 / 88.23 / 63.88	43.81 / 89.35 / 75.53	85.81 / 97.97 / 94.71

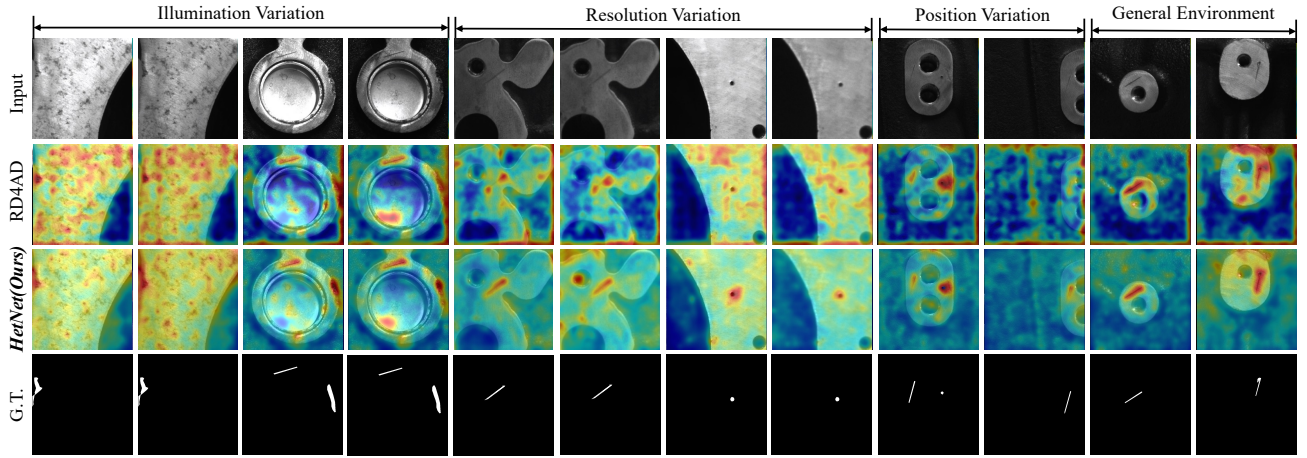


Fig. 3: Qualitative results on the MSC-AD dataset [15], demonstrating the efficacy of HetNet. From left to right, we present anomaly detection results for samples under varying illumination, resolution, and positioning conditions. Predictions made by HetNet robustly adapt to input disturbances and exhibit more stable performance across diverse environmental conditions. The lower image resolution or brightness only slightly affect the model accuracy.

the CNN encoder and student decoder, compute the differences between the pairs at different layers, and apply bilinear upsampling to restore the difference maps to the input image size. Finally, we aggregate the anomaly maps from all layers to generate the final anomaly localization score map. For anomaly detection, we take the maximum value from the anomaly score map as the image-level anomaly score.

3) Experiment Results and Discussions: We use the area under the receiver operating characteristic (AUROC) for evaluating image-level anomaly detection and pixel-level anomaly localization. To address AUROC’s bias toward large anomalies [28], we also utilize the per-region-overlap (PRO) metric for a fairer evaluation across different anomaly sizes.

Table.I presents the average results across different imaging conditions, calculated following [15]. HetNet outperforms SOTA methods in all categories on the MSC AD dataset, improving image-level AUROC by 18.46% over the second-best method [26] and nearly 40% over others. This indicates more accurate anomaly detection, likely due to the collaborative student network’s ability to delineate normal and abnormal feature boundaries on complex industrial

workpieces, without being influenced by environmental variations.

AUROC favors larger anomaly regions, while AUPRO provides a more balanced evaluation of anomalies of different sizes [28]. As shown in Table.I, HetNet achieves superior average pixel-level AUPRO results compared to SOTA methods, indicating its effectiveness in detecting and localizing small anomalies. Qualitative results in Fig.3 further demonstrate its capability in detecting metal surface defects in complex industrial environments.

B. Ablation Study

We conducted ablation experiments on the MSC-AD dataset to exhibit the effectiveness of each module in HetNet. Experiments were conducted on the difficult subset with 150 resolution classes under high and low illumination, as this subset is the most challenging and representative of real industrial environments. Results on additional datasets further evaluate our method’s generalization capability.

1) Teacher Network Structure: The first three rows of Table.II show the importance of the heterogeneous teacher

TABLE II: Ablation study results of different modules.

TE	ALGF	LMGN	I-AUROC	P-AUROC	P-AUPRO
CNN	✗	✗	42.02	86.22	69.59
Trans	✗	✗	49.78	43.80	58.62
HTE	✗	✗	80.98	96.93	91.76
HTE	✓	✗	83.46	97.18	92.30
HTE	✗	✓	84.02	97.23	92.36
HTE	✓	✓	84.20	97.30	92.85

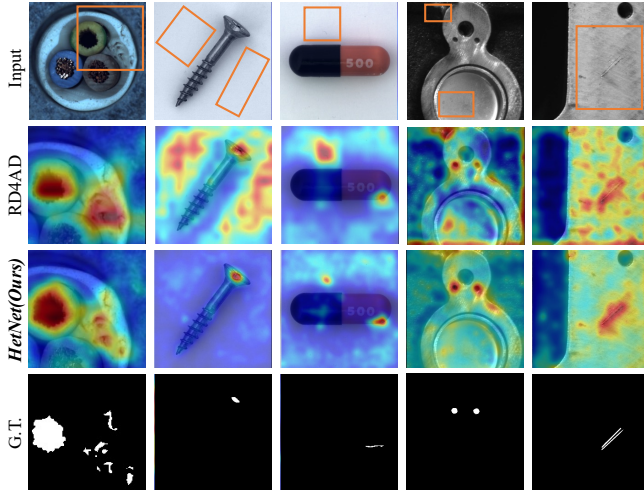


Fig. 4: Qualitative comparisons demonstrating HetNet’s effectiveness in reducing false positives on normal disruptive patterns. The highlighted regions in the first row show areas where baseline methods produce significant false positives or ambiguous predictions. First three columns are from MVTEC-AD [6], while last two columns are from MSC-AD [15].

encoder (HTE). Using only a standalone CNN or Transformer network results in lower performance than the heterogeneous teacher encoder. This validates the combination of Transformer and CNN in HTE.

2) Module Ablation Design: The last four rows of Table.II present results for different architecture configurations. (1) HetNet achieves strong performance even without the feature fusion and noise modules, indicating the effectiveness of HTE. (2) Performance improves with the addition of the ALGF and LMGN modules. (3) Including both modules yields the best results in anomaly detection and localization.

TABLE III: Ablation study results of different noise types.

Noise	I-AUROC	P-AUROC	P-AUPRO
✗	83.46	97.18	92.30
randn	83.89	97.27	92.76
mGds(Ours)	84.20	97.30	92.85

3) Choice of Noise Type: Table.III shows the impact of different noise types. Results show that introducing standard normal distribution noise (randn) slightly improves performance, but sampling noise from a multivariate Gaussian distribution (mGds) yields optimal performance, enhancing model robustness.

4) Results on Additional Datasets: As demonstrated in Table IV, the proposed HetNet achieves state-of-the-art

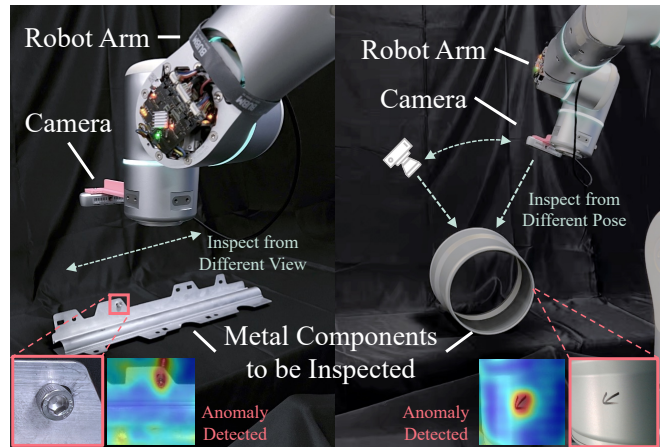


Fig. 5: The real-world environment setting.

performance across three diverse public benchmarks. On the MVTEC AD dataset, our approach attains the highest image-level AUC score of 99.19% and pixel-level PRO score of 94.63%, which can be attributed to the heterogeneous feature encoding mechanism that effectively captures both global semantic inconsistencies and local structural anomalies. For the more challenging VisA dataset, HetNet significantly outperforms existing methods with an I-AU of 96.19% and P-PRO of 94.06%. This substantial enhancement stems from our multi-scale feature fusion strategy that adaptively balances high-level semantic information with low-level textural details, particularly beneficial for the diverse anomaly types present in VisA. On the MPDD dataset, which features complex surface defects under varying illumination conditions, HetNet demonstrates competitive performance with the highest P-PRO score of 95.43% while maintaining strong results across other evaluation metrics. The consistent superiority across these datasets with distinct characteristics (controlled lighting in MVTEc, complex backgrounds in VisA, and illumination variations in MPDD) empirically validates the theoretical foundation of our approach: that heterogeneous feature interaction effectively bridges the representational gap between normal and anomalous patterns across different industrial inspection scenarios, leading to improved generalization capabilities without requiring domain-specific adaptations. More qualitative results can be found in Fig.4

C. Real Environment Experiments

As shown in Fig. 5, after validating HetNet’s effectiveness on public datasets, we deployed it in a real-world industrial inspection setting to detect surface defects on precision metal components. The detection platform integrates Flexiv Rizon 7-Axis Robot Arm equipped with Intel RealSense D415 camera, connected to a dedicated computing system. During the inspection process, the robotic arm strategically maneuvers the camera along different positions and angles of the metal components, enabling our system to capture comprehensive multi-view images. This dynamic capture approach inherently introduces one of the key challenges in industrial inspection—the varying appearance of surfaces

TABLE IV: Results on Additional datasets.

Method	MVTec AD			VisA			MPDD		
	I-AU	P-AU	P-PRO	I-AU	P-AU	P-PRO	I-AU	P-AU	P-PRO
DRAEM [35]	98.00	97.30	N	92.4	92.0	78.7	94.3	90.7	78.0
CFA [26]	99.17	98.15	94.44	92.0	84.3	55.1	92.3	94.8	83.2
CFLOW [21]	98.26	98.62	94.60	87.77	98.04	85.29	87.11	97.42	88.56
RD4AD [30]	98.46	97.81	93.93	92.4	96.1	93.0	95.3	98.7	95.2
HetNet(Ours)	99.19	98.04	94.63	96.19	98.78	94.06	92.76	98.57	95.43

under different viewing conditions—which aligns with our method’s robust feature extraction capabilities demonstrated on the benchmark datasets. The controlled movement of the camera also enables comprehensive detection of defects that would be imperceptible from a single viewpoint. Our HetNet algorithm operates on an Intel i7-8565u processor and a GeForce RTX 3080, utilizing approximately 1.5 GB of VRAM. The time cost for detecting a single image is only 0.27 s to 0.33 s, demonstrating high efficiency and meeting the speed requirements of industrial automated production lines. These practical deployment results validate HetNet’s potential for real-world application in high-precision manufacturing inspection scenarios where consistent performance across varying inspection conditions is critical.

V. CONCLUSIONS

In this work, we present HetNet, an approach to anomaly detection and localization in complex industrial environments. Our model learns the distribution of intricate normal patterns from data with local variations. We introduce three key components: a heterogeneous teacher encoder that exploits the complementary strengths of different networks, a fusion module to harmonize heterogeneous teacher-student networks, and a noise generator to introduce complex variation information, improving the model’s robustness to diverse inputs. Our method achieves state-of-the-art performance on mainstream benchmarks and proves its high practical value in real-world environment tests.

REFERENCES

- [1] G. Zhang, Y. Lu, X. Jiang, F. Yan, and M. Xu, “Context-aware adaptive weighted attention network for real-time surface defect segmentation,” *IEEE Transactions on Instrumentation and Measurement*, vol. 73, pp. 1–13, 2024.
- [2] A. Rasheed, B. Zafar, A. Rasheed, N. Ali, M. Sajid, S. H. Dar, U. Habib, T. Shehryar, and M. T. Mahmood, “Fabric defect detection using computer vision techniques: a comprehensive review,” *Mathematical Problems in Engineering*, vol. 2020, no. 1, p. 8189403, 2020.
- [3] F. Wang, G. Song, J. Mao, Y. Li, Z. Ji, D. Chen, and A. Song, “Internal defect detection of overhead aluminum conductor composite core transmission lines with an inspection robot and computer vision,” *IEEE Transactions on Instrumentation and Measurement*, vol. 72, pp. 1–16, 2023.
- [4] Y. Du, H. Chen, Y. Fu, J. Zhu, and H. Zeng, “Aff-net: A strip steel surface defect detection network via adaptive focusing features,” *IEEE Transactions on Instrumentation and Measurement*, vol. 73, pp. 1–14, 2024.
- [5] Y. Chen, Y. Ding, F. Zhao, E. Zhang, Z. Wu, and L. Shao, “Surface defect detection methods for industrial products: A review,” *Applied Sciences*, vol. 11, no. 16, p. 7657, 2021.
- [6] P. Bergmann, M. Fauser, D. Sattlegger, and C. Steger, “Mvtect-ad—a comprehensive real-world dataset for unsupervised anomaly detection,” in *Proceedings of the IEEE/CVF conference on computer vision and pattern recognition*, 2019, pp. 9592–9600.
- [7] P. Bergmann, S. Löwe, M. Fauser, D. Sattlegger, and C. Steger, “Improving unsupervised defect segmentation by applying structural similarity to autoencoders,” *arXiv preprint arXiv:1807.02011*, 2018.
- [8] I. Golan and R. El-Yaniv, “Deep anomaly detection using geometric transformations,” *Advances in neural information processing systems*, vol. 31, 2018.
- [9] D. Gong, L. Liu, V. Le, B. Saha, M. R. Mansour, S. Venkatesh, and A. v. d. Hengel, “Memorizing normality to detect anomaly: Memory-augmented deep autoencoder for unsupervised anomaly detection,” in *Proceedings of the IEEE/CVF conference on computer vision and pattern recognition*, 2019, pp. 1705–1714.
- [10] H. Park, J. Noh, and B. Ham, “Learning memory-guided normality for anomaly detection,” in *Proceedings of the IEEE/CVF conference on computer vision and pattern recognition*, 2020, pp. 14 372–14 381.
- [11] M. Salehi, N. Sadjadi, S. Baselizadeh, M. H. Rohban, and H. R. Rabiee, “Multiresolution knowledge distillation for anomaly detection,” in *Proceedings of the IEEE/CVF conference on computer vision and pattern recognition*, 2021, pp. 14 902–14 912.
- [12] G. Wang, S. Han, E. Ding, and D. Huang, “Student-teacher feature pyramid matching for anomaly detection,” *arXiv preprint arXiv:2103.04257*, 2021.
- [13] Q. Wan, L. Gao, X. Li, and L. Wen, “Unsupervised image anomaly detection and segmentation based on pretrained feature mapping,” *IEEE Transactions on Industrial Informatics*, vol. 19, no. 3, pp. 2330–2339, 2022.
- [14] C. Wang, W. Zhu, B.-B. Gao, Z. Gan, J. Zhang, Z. Gu, S. Qian, M. Chen, and L. Ma, “Real-iaid: A real-world multi-view dataset for benchmarking versatile industrial anomaly detection,” in *Proceedings of the IEEE/CVF Conference on Computer Vision and Pattern Recognition*, 2024, pp. 22 883–22 892.
- [15] Q. Zhao, Y. Wang, B. Wang, J. Lin, S. Yan, W. Song, A. Liotta, J. Yu, S. Gao, and W. Zhang, “Msc-ad: A multiscene unsupervised anomaly detection dataset for small defect detection of casting surface,” *IEEE Transactions on Industrial Informatics*, 2023.
- [16] A. Krizhevsky, I. Sutskever, and G. E. Hinton, “Imagenet classification with deep convolutional neural networks,” *Advances in neural information processing systems*, vol. 25, 2012.
- [17] N. Cohen and Y. Hoshen, “Sub-image anomaly detection with deep pyramid correspondences,” *arXiv preprint arXiv:2005.02357*, 2020.
- [18] K. Roth, L. Pemula, J. Zepeda, B. Schölkopf, T. Brox, and P. Gehler, “Towards total recall in industrial anomaly detection,” in *Proceedings of the IEEE/CVF conference on computer vision and pattern recognition*, 2022, pp. 14 318–14 328.
- [19] T. Defard, A. Setkov, A. Loesch, and R. Audigier, “Padim: a patch distribution modeling framework for anomaly detection and localization,” in *International Conference on Pattern Recognition*. Springer, 2021, pp. 475–489.
- [20] J. Bae, J.-H. Lee, and S. Kim, “Pni: Industrial anomaly detection using position and neighborhood information,” in *Proceedings of the IEEE/CVF conference on computer vision and pattern recognition*, 2023, pp. 6373–6383.
- [21] D. Gudovskiy, S. Ishizaka, and K. Kozuka, “Cflow-ad: Real-time unsupervised anomaly detection with localization via conditional normalizing flows,” in *Proceedings of the IEEE/CVF winter conference on applications of computer vision*, 2022, pp. 98–107.
- [22] D. Kim, S. Baik, and T. H. Kim, “Sanflow: Semantic-aware normalizing flow for anomaly detection,” *Advances in Neural Information Processing Systems*, vol. 36, pp. 75 434–75 454, 2023.
- [23] C.-L. Li, K. Sohn, J. Yoon, and T. Pfister, “Cutpaste: Self-supervised learning for anomaly detection and localization,” in *Proceedings of the IEEE/CVF conference on computer vision and pattern recognition*, 2021, pp. 9664–9674.

- [24] H. M. Schlüter, J. Tan, B. Hou, and B. Kainz, "Natural synthetic anomalies for self-supervised anomaly detection and localization," in *European Conference on Computer Vision*. Springer, 2022, pp. 474–489.
- [25] Z. Liu, Y. Zhou, Y. Xu, and Z. Wang, "Simplenet: A simple network for image anomaly detection and localization," in *Proceedings of the IEEE/CVF Conference on Computer Vision and Pattern Recognition*, 2023, pp. 20 402–20 411.
- [26] S. Lee, S. Lee, and B. C. Song, "Cfa: Coupled-hypersphere-based feature adaptation for target-oriented anomaly localization," *IEEE Access*, vol. 10, pp. 78 446–78 454, 2022.
- [27] G. Hinton, "Distilling the knowledge in a neural network," *arXiv preprint arXiv:1503.02531*, 2015.
- [28] P. Bergmann, M. Fauser, D. Sattlegger, and C. Steger, "Uninformed students: Student-teacher anomaly detection with discriminative latent embeddings," in *Proceedings of the IEEE/CVF Conference on Computer Vision and Pattern Recognition (CVPR)*, June 2020.
- [29] G. Wang, S. Han, E. Ding, and D. Huang, "Student-teacher feature pyramid matching for anomaly detection," *arXiv preprint arXiv:2103.04257*, 2021.
- [30] H. Deng and X. Li, "Anomaly detection via reverse distillation from one-class embedding," in *Proceedings of the IEEE/CVF conference on computer vision and pattern recognition*, 2022, pp. 9737–9746.
- [31] Z. Gu, L. Liu, X. Chen, R. Yi, J. Zhang, Y. Wang, C. Wang, A. Shu, G. Jiang, and L. Ma, "Remembering normality: Memory-guided knowledge distillation for unsupervised anomaly detection," in *Proceedings of the IEEE/CVF conference on computer vision and pattern recognition*, 2023, pp. 16 401–16 409.
- [32] X. Zhang, S. Li, X. Li, P. Huang, J. Shan, and T. Chen, "Destseg: Segmentation guided denoising student-teacher for anomaly detection," in *Proceedings of the IEEE/CVF Conference on Computer Vision and Pattern Recognition*, 2023, pp. 3914–3923.
- [33] F. Lu, X. Yao, C.-W. Fu, and J. Jia, "Removing anomalies as noises for industrial defect localization," in *Proceedings of the IEEE/CVF conference on computer vision and pattern recognition*, 2023, pp. 16 166–16 175.
- [34] X. Zhang, N. Li, J. Li, T. Dai, Y. Jiang, and S.-T. Xia, "Unsupervised surface anomaly detection with diffusion probabilistic model," in *Proceedings of the IEEE/CVF conference on computer vision and pattern recognition*, 2023, pp. 6782–6791.
- [35] V. Zavrtanik, M. Kristan, and D. Škočaj, "Draem-a discriminatively trained reconstruction embedding for surface anomaly detection," in *Proceedings of the IEEE/CVF conference on computer vision and pattern recognition*, 2021, pp. 8330–8339.
- [36] Z. You, K. Yang, W. Luo, L. Cui, Y. Zheng, and X. Le, "Adtr: Anomaly detection transformer with feature reconstruction," in *International Conference on Neural Information Processing*. Springer, 2022, pp. 298–310.
- [37] Z. You, L. Cui, Y. Shen, K. Yang, X. Lu, Y. Zheng, and X. Le, "A unified model for multi-class anomaly detection," *Advances in Neural Information Processing Systems*, vol. 35, pp. 4571–4584, 2022.
- [38] H. Guo, L. Ren, J. Fu, Y. Wang, Z. Zhang, C. Lan, H. Wang, and X. Hou, "Template-guided hierarchical feature restoration for anomaly detection," in *Proceedings of the IEEE/CVF conference on computer vision and pattern recognition*, 2023, pp. 6447–6458.
- [39] X. Yao, R. Li, Z. Qian, Y. Luo, and C. Zhang, "Focus the discrepancy: Intra-and inter-correlation learning for image anomaly detection," in *Proceedings of the IEEE/CVF conference on computer vision and pattern recognition*, 2023, pp. 6803–6813.
- [40] Y. Zhao, "Omnia: A unified cnn framework for unsupervised anomaly localization," in *Proceedings of the IEEE/CVF Conference on Computer Vision and Pattern Recognition*, 2023, pp. 3924–3933.
- [41] I. Goodfellow, J. Pouget-Abadie, M. Mirza, B. Xu, D. Warde-Farley, S. Ozair, A. Courville, and Y. Bengio, "Generative adversarial networks," *Communications of the ACM*, vol. 63, no. 11, pp. 139–144, 2020.
- [42] A. Vaswani, "Attention is all you need," *Advances in Neural Information Processing Systems*, 2017.
- [43] J. Ho, A. Jain, and P. Abbeel, "Denoising diffusion probabilistic models," *Advances in neural information processing systems*, vol. 33, pp. 6840–6851, 2020.
- [44] T. D. Tien, A. T. Nguyen, N. H. Tran, T. D. Huy, S. Duong, C. D. T. Nguyen, and S. Q. Truong, "Revisiting reverse distillation for anomaly detection," in *Proceedings of the IEEE/CVF conference on computer vision and pattern recognition*, 2023, pp. 24 511–24 520.
- [45] J. Guo, L. Jia, W. Zhang, H. Li, *et al.*, "Recontrast: Domain-specific anomaly detection via contrastive reconstruction," *Advances in Neural Information Processing Systems*, vol. 36, 2024.
- [46] J. Zhang, C. Wang, X. Li, G. Tian, Z. Xue, Y. Liu, G. Pang, and D. Tao, "Learning feature inversion for multi-class anomaly detection under general-purpose coco-ad benchmark," *arXiv preprint arXiv:2404.10760*, 2024.
- [47] M. Wieler and T. Hahn, "Weakly supervised learning for industrial optical inspection," in *DAGM symposium in*, vol. 6, 2007, p. 11.
- [48] X. Tao, D. Zhang, Z. Wang, X. Liu, H. Zhang, and D. Xu, "Detection of power line insulator defects using aerial images analyzed with convolutional neural networks," *IEEE Transactions on Systems, Man, and Cybernetics: Systems*, 2018.
- [49] T. Bao, J. Chen, W. Li, X. Wang, J. Fei, L. Wu, R. Zhao, and Y. Zheng, "Miaid: A maintenance inspection dataset for unsupervised anomaly detection," in *Proceedings of the IEEE/CVF conference on computer vision and pattern recognition*, 2023, pp. 993–1002.
- [50] K. Song and Y. Yan, "A noise robust method based on completed local binary patterns for hot-rolled steel strip surface defects," *Applied Surface Science*, vol. 285, pp. 858–864, 2013.
- [51] H. Han, R. Yang, S. Li, R. Hu, and X. Li, "Ssgd: A smartphone screen glass dataset for defect detection," in *ICASSP 2023-2023 IEEE International Conference on Acoustics, Speech and Signal Processing (ICASSP)*. IEEE, 2023, pp. 1–5.
- [52] P. Mishra, R. Verk, D. Fornasier, C. Piciarelli, and G. L. Foresti, "Vt-adl: A vision transformer network for image anomaly detection and localization," in *2021 IEEE 30th International Symposium on Industrial Electronics (ISIE)*. IEEE, 2021, pp. 01–06.
- [53] P. Bergmann, K. Batzner, M. Fauser, D. Sattlegger, and C. Steger, "Beyond dents and scratches: Logical constraints in unsupervised anomaly detection and localization," *International Journal of Computer Vision*, vol. 130, no. 4, pp. 947–969, 2022.
- [54] Y. Zou, J. Jeong, L. Pemula, D. Zhang, and O. Dabeer, "Spot-the-difference self-supervised pre-training for anomaly detection and segmentation," in *European Conference on Computer Vision*. Springer, 2022, pp. 392–408.
- [55] H. Bai, S. Mou, T. Likhomanenko, R. G. Cinbis, O. Tuzel, P. Huang, J. Shan, J. Shi, and M. Cao, "Vision datasets: A benchmark for vision-based industrial inspection," *arXiv preprint arXiv:2306.07890*, 2023.
- [56] J. Zhang, R. Ding, M. Ban, and L. Dai, "Pku-goodsad: A supermarket goods dataset for unsupervised anomaly detection and segmentation," *IEEE Robotics and Automation Letters*, 2024.
- [57] D. Yang, Y. Cui, Z. Yu, and H. Yuan, "Deep learning based steel pipe weld defect detection," *Applied Artificial Intelligence*, vol. 35, no. 15, pp. 1237–1249, 2021.
- [58] C. S. Tsang, H. Y. Ngan, and G. K. Pang, "Fabric inspection based on the elo rating method," *Pattern Recognition*, vol. 51, pp. 378–394, 2016.
- [59] D. Tabernik, S. Šela, J. Skvarč, and D. Škočaj, "Segmentation-based deep-learning approach for surface-defect detection," *Journal of Intelligent Manufacturing*, vol. 31, no. 3, pp. 759–776, 2020.
- [60] J. Božič, D. Tabernik, and D. Škočaj, "Mixed supervision for surface-defect detection: From weakly to fully supervised learning," *Computers in Industry*, vol. 129, p. 103459, 2021.
- [61] Y. Huang, C. Qiu, and K. Yuan, "Surface defect saliency of magnetic tile," *The Visual Computer*, vol. 36, no. 1, pp. 85–96, 2020.
- [62] J. Deng, W. Dong, R. Socher, L.-J. Li, K. Li, and L. Fei-Fei, "Imagenet: A large-scale hierarchical image database," in *2009 IEEE conference on computer vision and pattern recognition*. Ieee, 2009, pp. 248–255.
- [63] S. Jezek, M. Jonak, R. Burget, P. Dvorak, and M. Skotak, "Deep learning-based defect detection of metal parts: evaluating current methods in complex conditions," in *2021 13th International congress on ultra modern telecommunications and control systems and workshops (ICUMT)*. IEEE, 2021, pp. 66–71.
- [64] S. Zagoruyko, "Wide residual networks," *arXiv preprint arXiv:1605.07146*, 2016.
- [65] Z. Liu, Y. Lin, Y. Cao, H. Hu, Y. Wei, Z. Zhang, S. Lin, and B. Guo, "Swin transformer: Hierarchical vision transformer using shifted windows," in *Proceedings of the IEEE/CVF conference on computer vision and pattern recognition*, 2021, pp. 10 012–10 022.
- [66] D. P. Kingma, "Adam: A method for stochastic optimization," *arXiv preprint arXiv:1412.6980*, 2014.